Virtual Parity-Time Symmetry

Huanan Li,[1] Ahmed Mekawy,[1,2] Alex Krasnok,[1] and Andrea Alù[1,2,3,*]
[1]Photonics Initiative, Advanced Science Research Center, City University of New York, New York, New York 10031, USA
[2]Department of Electrical Engineering, City College of The City University of New York, New York, New York 10031, USA
[3]Physics Program, Graduate Center, City University of New York, New York, New York 10016, USA

(Received 5 November 2019; accepted 23 April 2020; published 14 May 2020)

Parity-time (PT) symmetry has recently been opening exciting directions in photonics, yet the required careful balance of loss and gain has been hindering its widespread applicability. Here, we propose a gain-free route to PT symmetry by extending it to complex-frequency excitations that can mimic gain in passive systems. Based on the concept of virtual absorption, extended here to implement also virtual gain, we implement PT symmetry in the complex-frequency plane and realize its landmark effects, such as broken phase transitions, anisotropic transmission resonances, and laser-absorber pairs, in a fully passive, hence inherently stable, system. These results open a path to establish PT symmetry and non-Hermitian physics in passive platforms.

DOI: 10.1103/PhysRevLett.124.193901

Non-Hermitian wave physics has been gaining increased attention since the discovery and demonstration of its intriguing wave phenomena, such as single-mode lasers [1–2], unidirectional invisibility [3–5], PT-symmetric laser-absorber pairs [6–8], anisotropic transmission resonances (ATRs) [9–10], broken phase regimes, and exceptional points (EPs) [11–15]. These novel phenomena have been discovered within the context of parity-time (PT) symmetry [16], a special type of symmetry that satisfies inversion upon space and time, stemming from pioneering works in theoretical quantum physics [17–19]. PT symmetry was later fruitfully applied to classical settings [15], from photonics [4], electronics [20–21], plasmonics [22–23], acoustics [24], and metamaterials [25–27].

PT-symmetric systems in classical wave physics require the presence of gain. In optics, for example, PT symmetry implies that the complex refractive index satisfies $n(\boldsymbol{r}) = n^*(-\boldsymbol{r})$, resulting in a balanced gain-loss profile $\mathrm{Im}n(-\boldsymbol{r}) = -\mathrm{Im}n(\boldsymbol{r})$. This requirement has hindered several possibilities to implement and verify these concepts in practical devices due to the challenge of implementing sufficient gain in photonics and the incurrence of gain-induced instabilities [28–31]. In an attempt to overcome these issues, it has been argued that a weak form of PT symmetry can be somewhat mimicked in purely lossy systems [32–34].

Consider, for instance, the simplest case of two optical modes with the same resonance frequency u_0, different decay rates $\gamma_0 + \gamma$ and $\gamma_0 - \gamma$, $\gamma_0 > \gamma > 0$, and a real coupling coefficient κ. The dynamics of the coupled system are described by

$$\frac{d}{dt}|\Psi\rangle = jH_0|\Psi\rangle, \qquad |\Psi\rangle = \begin{pmatrix} \psi_L \\ \psi_R \end{pmatrix}, \tag{1}$$

with effective Hamiltonian $H_0 = \begin{pmatrix} u_0+j(\gamma_0+\gamma) & \kappa \\ \kappa & u_0+j(\gamma_0-\gamma) \end{pmatrix}$, where ψ_α, $\alpha = L$, R is the amplitude of the α-mode normalized such that $|\psi_\alpha|^2$ represents its energy. An analog to PT symmetry may be revealed by offsetting the average decay rate, i.e., after the transformation $\begin{pmatrix} \psi_L \\ \psi_R \end{pmatrix} = e^{-\gamma_0 t}\begin{pmatrix} \psi'_L \\ \psi'_R \end{pmatrix}$, for which the Hamiltonian becomes $H_0^{PT} = \begin{pmatrix} u_0+j\gamma & \kappa \\ \kappa & u_0-j\gamma \end{pmatrix}$, respecting PT symmetry with parity operator $P = \begin{pmatrix} 0 & 1 \\ 1 & 0 \end{pmatrix}$ and time-reversal operator T indicating complex conjugation. In this framework, the eigenvalue spectra $\omega_\pm^{PT} = u_0 \pm \sqrt{\kappa^2 - \gamma^2}$ sustain a broken phase regime as γ crosses the EP at $\gamma_{\mathrm{EP}} = \kappa$. This tool has been shown to verify some of the properties of PT symmetry in passive systems [35], but it implies global attenuation and requires postprocessing to actually observe the desired scattering phenomena. More complex PT-symmetric responses, such as ATRs or laser-absorber pairs, are not available in this framework because of passivity and power conservation.

In a different context, our group has recently introduced the concept of "virtual absorption" [36–38], based on which it is possible to mimic absorption in a system without loss by exciting it with nonmonochromatic growing waves, enabling efficient energy trapping and, when combined with nonlinearities, providing a powerful tool for storage and release beyond the time-bandwidth limit [39]. Here, we extend this concept to "virtual gain" and realize

"virtual PT symmetry" in an inherently passive and stable material platform that oscillates at complex frequencies. Our Letter extends the concept of PT symmetry in the complex-frequency plane and enables observation of all the properties of PT-symmetric systems without requiring active elements, but instead considering complex-frequency excitations.

Virtual gain.—Dual to virtual absorption, virtual gain can be achieved by exciting a passive system with a signal decaying in time. Consider a balanced transmission line (TL), characterized by uniform loss $\gamma_0 > 0$ [40] (see Supplemental Material [41]) and excited by a voltage signal $v_0(z,t) = V_0^+ e^{j\omega_c t - j\beta z}$ oscillating at complex frequency $\omega_c = \omega + j\sigma$, with $0 < \sigma \ll \omega$. As the decaying signal flows through the TL, the time-average power flow $J(z,t) = (|V_0^+|^2/2Z_0)e^{-2\sigma t + 2(\sigma-\gamma_0)z/v_p}$, where Z_0 is the characteristic impedance and v_p is the phase velocity. In the monochromatic regime ($\sigma = 0$), the signal decays along the line at a rate dictated by the TL loss [Fig. 1(a)]. However, if the decay rate σ of our signal is equal to the uniform loss γ_0, the power flow does not depend on z at any instant in time. Further, when $\sigma > \gamma_0$, the power flow $J(z,t)$ grows along the propagation direction, up to the signal precursor, mimicking gain in a fully passive system.

Virtual PT symmetry.—More complicated is the implementation of balanced gain and loss at the same complex frequency. We achieve virtual PT symmetry by loading the TL with a pair of suitably tailored coupled resonators [see Fig. 2(a)]. We design the system such that, after transient it reaches a quasistationary state, in which reflected and transmitted signals all oscillate in time following the same complex-frequency dynamics. To describe this response, we can use temporal coupled-mode theory (CMT) [42]

$$\frac{d}{dt}|\Psi\rangle = (jH_0 - \Gamma)|\Psi\rangle + D^T|s_+\rangle,$$
$$|s_-\rangle = -|s_+\rangle + D|\Psi\rangle, \tag{2}$$

where the input vector $|s_+\rangle = \binom{L^{(i)}}{R^{(i)}}$ is formed by power-normalized amplitudes $L^{(i)}$ and $R^{(i)}$ for incoming waves from left and right ports, and similarly, the output vector $|s_-\rangle = \binom{L^{(o)}}{R^{(o)}}$ for outgoing waves; the 2×2 real matrix D describes the coupling between ports and the two modes, and the matrix $\Gamma = \frac{1}{2}D^+D$ accounts for the decay into the ports. For complex-frequency excitation $|s_+\rangle = e^{-\sigma t + j\omega t}|s_+^0\rangle$ with decay rate $\sigma = \gamma_0$, i.e., balancing the average loss γ_0 of H_0 in Eq. (1), the scattering matrix S connecting the output in the quasistationary state with the input via $|s_-\rangle = S|s_+\rangle$ reads

$$S(\omega) = -I_2 + jD\frac{1}{H_0^{PT} + j\Gamma - \omega}D^T, \tag{3}$$

where I_2 is the 2×2 identity matrix, and the PT-symmetric Hamiltonian H_0^{PT} derived above determines the internal dynamics. The S matrix in (3) obeys the relation $PTS(\omega)PT = S^{-1}(\omega), \omega \in \mathcal{R}$, identical to a PT-symmetric system, despite the absence of gain. Hence, in the quasistationary state we expect this system to support all the exotic scattering phenomena expected in a system with balanced loss and gain, such as ATR and CPA-lasing [7–9].

The overall temporal response is defined by the interplay between the transient process, related to the initial state $|\Psi(0)\rangle$ and the quasistationary process determined by the S matrix. The entire dynamics is revealed solving Eq. (2): the outgoing waves

$$|s_-\rangle = S|s_+\rangle + De^{jH_{\text{eff}}^0 t}D^{-1}[D|\Psi(0)\rangle - (S+I_2)|s_+^0\rangle], \tag{4}$$

where the eigenvalues of the matrix $H_{\text{eff}}^0 = H_0 + j\Gamma$ represent the decay rates of the transient process. The quasistationary response is governed by the first term on the right-hand side of Eq. (4), whereas the transient process is described by the second term, associated with the initial state $|\Psi(0)\rangle$ of the system and the initial amplitude $|s_+^0\rangle$ of the impinging waves. To observe virtual PT symmetry, we carefully control the synergy between these two processes.

Virtual phase transition.—We implement these ideas in a tailored electronic circuit [Fig. 2(a)]. The circuit is composed of two coupled parallel RLC circuits with differential conductance G_L and G_R. Their coupling is controlled

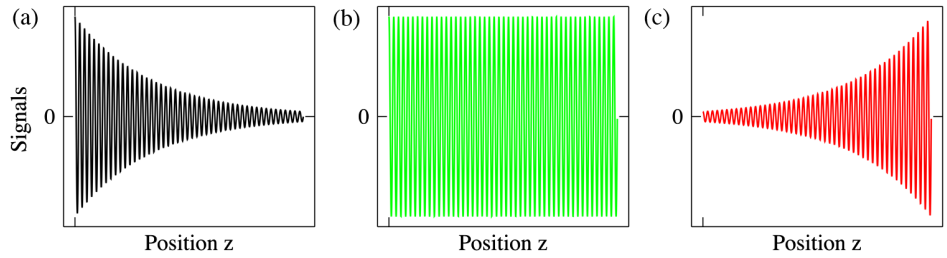

FIG. 1. Virtual gain: instantaneous signals in the quasistationary regime versus position z in a TL with uniform loss γ_0, when the signal decay rate (a) $\sigma = 0$, (b) $\sigma = \gamma_0$, and (c) $\sigma > \gamma_0$.

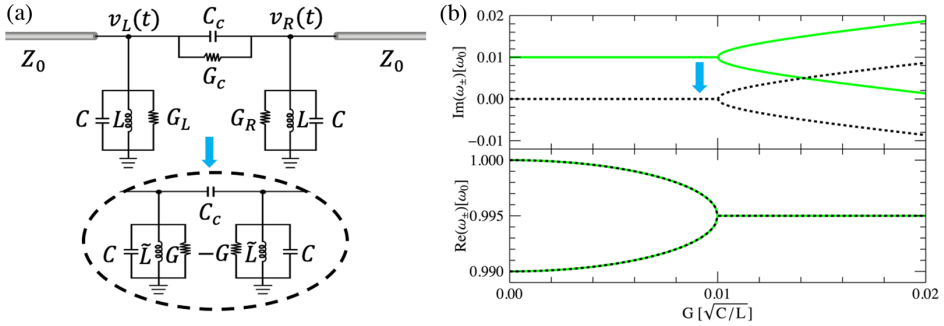

FIG. 2. (a) Schematic of a virtual PT-symmetric circuit. In its quasistationary state, the system is mapped onto a PT-symmetric circuit (inside the dashed circle) consisting of gain and loss balanced parallel $\tilde{L}RC$ resonators, with resistance $\pm R = \pm 1/G$ and renormalized inductance $\tilde{L} = L(1 + \gamma_0^2/\omega_{PT}^2)$. (b) The eigenvalue spectrum of the effective Hamiltonian of the system in (a) as a function of the Hermiticity parameter G. In the quasistationary state, these curves (solid green lines) are mapped onto the dashed lines, corresponding to a PT-symmetric transition. Here, $\hat{\gamma}_0 = \hat{c} = 0.01$.

by the capacitance C_c in parallel with conductance G_c. Input signals are fed into the circuit by TLs with impedance Z_0. Virtual PT symmetry is achieved for $|s_+\rangle = e^{-\gamma_0 t + j\omega t}|s_+^0\rangle$ when $\omega = \omega_{PT} \sim \omega_0 = 1/\sqrt{LC}$; in this framework, the Hermiticity parameter G is embedded in $G_{L/R} = \pm G + \{C + 1/[L(\omega_{PT}^2 + \gamma_0^2)]\}\gamma_0$, and we set $G_c = \gamma_0 C_c$. Correspondingly, as the system reaches the quasistationary state, it is fully analogous to the effective PT-symmetric circuit [see Fig. 2(a)] consisting of balanced gain and loss with resistances $\pm R = \pm 1/G$ and renormalized inductance $\tilde{L} = L(1 + \gamma_0^2/\omega_{PT}^2)$ [43]. The pair of resonators is capacitively coupled via C_c. Schelkunoff was the first to notice [44] that the impedance is an attribute of both the medium and the wave that excites it. Here, by tailoring the temporal profile of the impinging wave, we effectively implement balanced gain and loss in a fully passive circuit.

By exciting the system around the complex frequency $\omega_c = \omega + j\gamma_0$ with $\omega \sim \omega_0$ and $\hat{\gamma}_0 \equiv \gamma_0/\omega_0 \to 0$, and assuming that the coupling strengths $\hat{\varepsilon} = (1/Z_0)\sqrt{L/C}$ between the TLs and the circuit and $\hat{c} = C_c/C$ between the resonators are weak, of order $O(\hat{\gamma}_0)$, and that the internal loss of the resonators are small, $\hat{\gamma}_{L/R} \equiv G_{L/R}/(2C\omega_0) \leq O(\hat{\gamma}_0)$, the temporal CMT in Eq. (2) is applicable up to first order with respect to $\hat{\gamma}_0$ (see Supplemental Material [41]), and we can identify the parameters in Eq. (2) as $u_0 = \omega_0(1 - \frac{1}{2}\hat{c})$, $\kappa = \omega_0 \frac{1}{2}\hat{c}$, $\gamma_0 = (\omega_0/2)(\hat{\gamma}_L + \hat{\gamma}_R)$, $\gamma = (\omega_0/2)(\hat{\gamma}_L - \hat{\gamma}_R)$, and $D = \sqrt{\omega_0 \hat{\varepsilon}} I_2$. A phase transition determined by H_0 for the passive circuit [green lines in Fig. 2(b)] becomes a PT-symmetric phase transition [dashed lines] determined by H_0^{PT}. Indeed, the eigenvalues of S in Eq. (3) transition from being unimodular to a pair with reciprocal moduli [9,45].

To complete the analogy and demonstrate that our circuit is PT symmetric at the complex frequency, we derive the relation between voltages $v_{L/R}(t)$ at the left-right node [Fig. 2(a)] and mode amplitudes ψ_α, $\alpha = L$, R in Eq. (2),

$$\begin{pmatrix} v_\alpha \\ i_\alpha \end{pmatrix} = \frac{1}{\sqrt{2C}} \begin{pmatrix} 1 & 1 \\ j\omega_0 & -j\omega_0 \end{pmatrix} \begin{pmatrix} \psi_\alpha \\ \psi_\alpha^* \end{pmatrix}, \tag{5}$$

and between the incoming and outgoing voltage $v_\alpha^\pm$ at node $\alpha = L$, R and the input and output in Eq. (2) [41]

$$v_\alpha^\pm = \sqrt{\frac{Z_0}{2}}[\alpha^{(i/o)} + (\alpha^{(i/o)})^*]. \tag{6}$$

Virtual ATR.—Since at the chosen complex frequency our circuit is PT symmetric, we expect that its response supports all the exotic wave phenomena associated with PT symmetry. Particularly, as the system reaches the quasistationary state, we observe an ATR, i.e., a response for which the reflectance from one port is zero, $|S_{11}|^2 = 0$ at $\omega = \omega_{PT} = \omega_0(1 + \hat{\delta}) \in \mathcal{R}$, yielding

$$\hat{\varepsilon} = (\hat{\gamma}_L - \hat{\gamma}_R) \pm \sqrt{-4\hat{\delta}(\hat{c} + \hat{\delta})} \tag{7}$$

when we employ Eq. (3). PT symmetry ensures that $|S_{12}|^2 = |S_{21}|^2 = 1$ and generally $|S_{22}|^2 \neq 0$. Indeed, from Eq. (3) we find $|S_{22}|^2 = 4(\hat{\gamma}_L - \hat{\gamma}_R)^2/\hat{c}^2$.

To verify this response, we need to minimize the transient process, so that the system reaches quickly the quasistationary state. Therefore, we calculate the decay rates γ_{tran} of the transient process, given by the imaginary part of the two eigenvalues of H_{eff}^0. For a given value of $|S_{22}|^2$, the condition that maximizes the decay rate $\gamma_{\text{tran}}^<$ of the eigenmode that lives longer is given by $\hat{\delta} = -\frac{1}{2}\hat{c}$, $\hat{\gamma}_R = 0$, $\hat{\varepsilon} = \hat{\gamma}_L + \hat{c}$, yielding

$$\gamma_{\text{tran}}^< = \gamma_0 \left[2 + \frac{2}{|S_{22}|} - \text{Re}\sqrt{1 - \frac{4}{|S_{22}|^2}}\right], \tag{8}$$

corresponding to the fastest possible transient decay for given $|S_{22}|$. This quantity monotonically decreases with

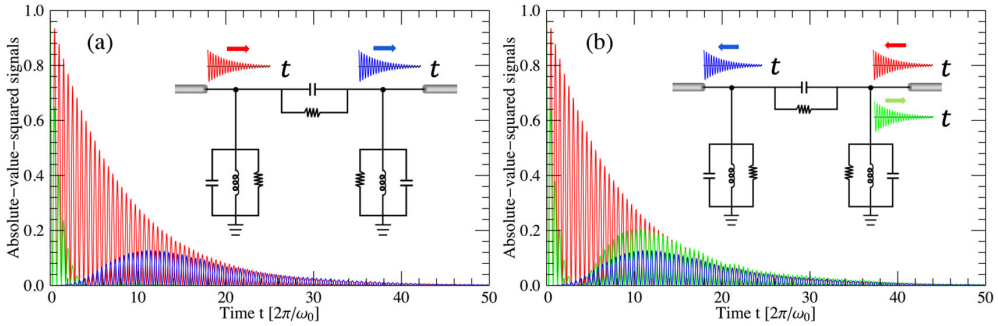

FIG. 3. Demonstration of virtual ATR. Time-dependent signals $v_L^+(t) = v_R^+(t)$ incident from (a) the left and (b) right port. (a),(b) We plot incident (red), reflected (green), and transmitted signals (blue). (Insets) Operation sketches in the quasistationary state. Here, $\omega_0 = 2\pi \times 50$ MHz, $L = 10$ nH, and $\hat{\gamma}_0 = 0.01$. Thus, $C = 1/(L\omega_0^2)$ and $\hat{\gamma}_R = 0$, $\hat{\varepsilon} \approx \hat{\gamma}_L + \hat{c}$, $\hat{\gamma}_L = \hat{\gamma}_0\{1 + 1/[(1+\hat{\delta})^2 + \hat{\gamma}_0^2]\}$, $\hat{\delta} = -\frac{1}{2}\hat{c}$, and $\hat{c} \approx 4\hat{\gamma}_0$ for ATR with $|S_{22}| = 1$. In addition, $G_1 = 2\hat{\gamma}_L\sqrt{C/L}$, $G_2 = 0$, $C_c = \hat{c}C$, $G_c = \hat{\gamma}_0\hat{c}\sqrt{C/L}$, $Z_0 = \sqrt{L/C}/\hat{\varepsilon}$, and the input signals have $\gamma_0 = \hat{\gamma}_0\omega_0$ and $\omega_{PT} = (1+\hat{\delta})\omega_0$.

$|S_{22}|$, hence a larger reflection contrast requires a larger contribution from the transient process. We numerically demonstrate a virtual ATR with $|S_{22}| = 1$, for which $\gamma_{\text{tran}}^{<} = 4\gamma_0$. The virtual ATR occurs in the PT-symmetric phase since $(|S_{11}|^2 + |S_{22}|^2)/2 - |S_{12}|^2 < 1$, which, from a spectrum analysis of the S matrix in Eq. (3), corresponds to the symmetric phases [9].

In Fig. 3, we perform time-domain scattering simulations of the optimized system, for $\omega_0 = 2\pi \times 50$ MHz, $L = 10$ nH, and $\hat{\gamma}_0 = 0.01$, yielding $Z_0 = \omega_0 L/\hat{\varepsilon} \approx 52\ \Omega$, where $\hat{\varepsilon} \approx 6\hat{\gamma}_0$, since we have $\hat{\varepsilon} = \hat{\gamma}_L + \hat{c}$, $\hat{c} = 2\hat{\gamma}_L$, and $\hat{\gamma}_L \approx 2\hat{\gamma}_0$. The initial voltage and current across capacitor and inductor in each resonator are set to zero. In Fig. 3(a), at $t = 0$ we send an input signal (red curve) from the left port and measure the (normalized) reflected signal $|v_L^-(t)|^2/|v_L^+(0)|^2$ (green), which rapidly decays to zero after a short transient. In contrast, the transmitted signal $|v_{L\to R}(t)|^2/|v_L^+(0)|^2$ (blue) grows and finally decays in perfect sync with the input signal as the system reaches the quasistationary state, confirming unitary transmission. Strikingly different is the response when sending the same signal from the right port [Fig. 3(b)]: the reflected voltage decays first due to the same transient process, but then picks up energy, and in the quasistationary state follows the excitation since $|S_{22}| = 1$. The transmitted signal follows the same trend as in Fig. 3(a) due to reciprocity. During the quasistationary state, at any instant in time, the total time-averaged power flowing out of the system is twice the incident one in this scenario [see inset in Fig. 3(b)], mimicking gain. Remarkably, we achieve this phenomenon in a purely passive system, where (virtual) gain is enabled by the reactive energy stored at earlier times in the system, and the suitable complex-frequency excitation.

Virtual absorber laser.—Another landmark feature of PT-symmetric systems is the realization of an absorber laser [6,7]. Here, we implement a virtual version of this phenomenon in a passive circuit. We require that the quasistationary scattering matrix S in Eq. (3) possesses a pair of eigenvalues going to zero and infinity, respectively, and thus the virtual absorber laser should operate in its PT-broken phase. This stringent requirement is fulfilled when the zero and pole of the S matrix coalesce at $\omega = \omega_{PT} = \omega_0(1 - \frac{1}{2}\hat{c})$, achieved in our circuit when $\hat{\delta} = -\frac{1}{2}\hat{c}$, as γ reaches the threshold value $\gamma_{\text{th}} = \frac{1}{2}\omega_0\sqrt{\hat{\varepsilon}^2 + \hat{c}^2}$. Indeed, when $\omega = \omega_{PT}$ and $\gamma \sim \gamma_{\text{th}}$, the eigenvalues $s_\pm$ of the S matrix are $s_+ = 1/s_-^* \approx -[\sqrt{\hat{\varepsilon}^2 + \hat{c}^2}/(\omega_0\hat{\varepsilon}^2)](\gamma - \gamma_{\text{th}})$.

In a conventional PT-symmetric laser absorber, lasing occurs when the Hermiticity parameter reaches the lasing threshold, beyond which the system becomes unstable. For the same system, coherent perfect absorption (CPA) can be achieved when the excitation matches the eigenvector $|s_{+,\text{CPA}}^0\rangle$ corresponding to the zero eigenvalue. In our scenario, the analog of lasing corresponds to the decay of the system into its quasinormal mode, sustained by the initial energy stored in the resonators. Virtual CPA, however, requires inputs with the same decay rate as the transient of the virtual lasing mode, hence it may be difficult to observe. Therefore, we employ monochromatic waves at ω_{PT} before $t = 0$ to prepare the system in order to have suitable initial states, so that the transient response is suppressed. From Eq. (4), the initial state required to avoid the transient is $|\Psi(0)\rangle = D^{-1}(S + I_2)|s_+^0\rangle$ [46], which is reached at $t = 0$ by exciting the system with $|s_+^P(t)\rangle = e^{j\omega_{PT}t}|s_+^{P,0}\rangle$ for $t \le 0$, and amplitude

$$|s_+^{P,0}\rangle = \left[\left(1 + \frac{\hat{\gamma}_0}{\hat{\varepsilon}}\right) + \frac{\hat{\gamma}_0}{\hat{\varepsilon}}S(\omega_{PT})\right]|s_+^0\rangle. \tag{9}$$

In this preparation stage, $|s_-^P(t)\rangle = e^{j\omega_{PT}t}|s_-^{P,0}\rangle$ with

$$|s_-^{P,0}\rangle = \left[\left(1 - \frac{\hat{\gamma}_0}{\hat{\varepsilon}}\right)S(\omega_{PT}) - \frac{\hat{\gamma}_0}{\hat{\varepsilon}}\right]|s_+^0\rangle. \tag{10}$$

In Fig. 4, we study the virtual CPA laser around the threshold γ_{th}, i.e., $\gamma = \gamma_{\text{th}}(1 - \hat{\delta}_\gamma)$. Interestingly, in contrast

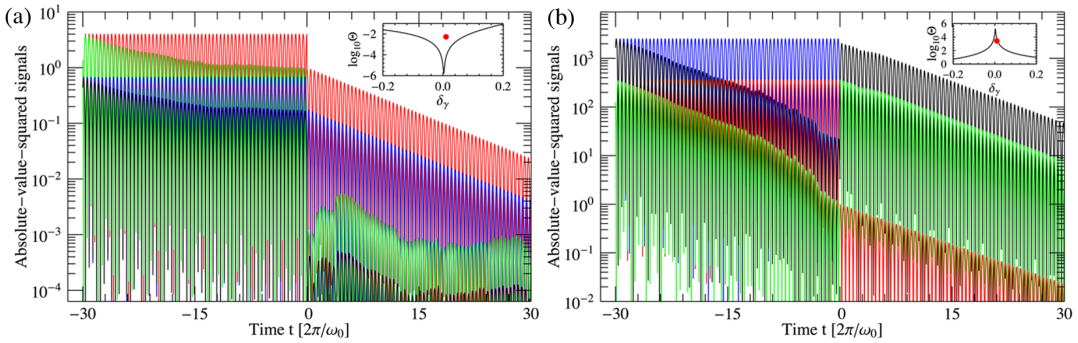

FIG. 4. Demonstration of absorption and amplification in a virtual CPA laser around its threshold. The initial state $|\Psi(t=0)\rangle$ is prepared by monochromatic excitation before $t=0$, injected from left (red curve) and right ports (blue). Time-domain reflected waves at the left (green) and right (black) ports are also shown. (a) Virtual CPA after $t=0$. (b) Virtual lasing. Here, $\hat{\delta}=-\frac{1}{2}\hat{c}$, $\hat{\gamma}_{L/R}\approx\hat{\gamma}_0\pm(\gamma_{\rm th}/\omega_0)(1-\hat{\delta}_\gamma)$ with detuning $\hat{\delta}_\gamma=0.01$, and $\hat{c}=\hat{\varepsilon}=\hat{\gamma}_0=0.01$. We choose $\omega_0=2\pi\times 50$ MHz, $L=10$ nH, and other circuit elements are determined as in Fig. 3. (Insets) The overall output power Θ versus $\hat{\delta}_\gamma$, confirming lasing and antilasing after $t=0$. Red dots indicate the result in the main panels.

to conventional CPA laser, our passive system allows exploring regimes beyond the threshold $\gamma_{\rm th}$ without incurring instabilities. Fixing $\hat{c}=\hat{\varepsilon}=\hat{\gamma}_0$, passivity $\hat{\gamma}_{L/R}\geq 0$ determines $\hat{\delta}_\gamma\geq 1-\sqrt{2}$, which crosses the threshold value at $\hat{\delta}_\gamma=0$. In the figure, we choose $\omega_0=2\pi\times 50$ MHz, $L=10$ nH, and $\hat{\gamma}_0=\hat{\delta}_\gamma=0.01$.

In Fig. 4(a), we excite the structure with the CPA eigenvector $|s_+^{\rm CPA}\rangle=e^{-\gamma_0 t+j\omega_{PT}t}|s_{+,\rm CPA}^0\rangle$, $|s_{+,\rm CPA}^0\rangle=(1,j\{-\hat{c}^2+[(2\gamma/\omega_0)-\hat{\varepsilon}]^2\}/(2\hat{c}\,\hat{\varepsilon}))^T$ after $t=0$ (red and blue lines). The system immediately reaches the quasistationary CPA state, without a transient. Indeed, the output curves (green, black) suddenly yield very small values. Consistent with Eq. (10), when $S(\omega_{PT})|s_{+,\rm CPA}^0\rangle=0$ and $\hat{\varepsilon}=\hat{\gamma}_0$, the reflectance at time $t=0^-$ due to the incoming monochromatic waves approaches the stationary value $|s_-^{P,0}\rangle$, which matches the incoming decaying signals at time $t=0^+$. In the inset, we show the effect of the detuning $\hat{\delta}_\gamma$ on the overall output signals Θ, i.e., the ratio of total outgoing to incoming intensity. The red dot indicates the result of the main panel at time $t/(2\pi/\omega_0)=15$, in which the absorption is limited to a finite value due to parasitics in realistic simulations, whereas the black curve is for ideal conditions (see Supplemental Material [41]). The scenario drastically changes if we consider the input $|s_+^0\rangle=(1\quad 0)^T$. As shown in Fig. 4(b), in this case the outgoing waves (green, black) are significantly larger than the incident one (red). The corresponding Θ coefficient, i.e., the red dot, with the predicted Θ versus $\hat{\delta}_\gamma$ for ideal conditions, confirms virtual lasing. Equation (9) ensures that when $\hat{\varepsilon}=\hat{\gamma}_0$, $|s_+^{P,0}\rangle\approx|s_-^0\rangle\equiv S(\omega_{PT})|s_+^0\rangle$ near the virtual lasing threshold, confirmed by our simulations. The reflected signal $|s_-^{P,0}\rangle$ is suppressed at $\hat{\varepsilon}=\hat{\gamma}_0$, following Eq. (10).

Conclusions.—In this Letter, we have shown that nonmonochromatic excitations oscillating at complex frequencies enable the implementation of PT symmetry in a fully passive system. We demonstrated transitions from real to broken phases, ATR and CPA-laser operations in a realistic circuit configuration without the need of active elements, ensuring passivity and stability, which enables exploring regimes beyond the lasing threshold. Practical demonstrations prefer high-Q resonators with small damping, enabling more easily quasistationary responses without fast decays of the signal. We believe that our results may inspire the realization of PT-symmetric and non-Hermitian physics in a variety of passive photonic, phononic, and electronic systems, enabling an interesting playground for classical and quantum optical phenomena without the need of stringent requirements on gain.

We thank Professor Tsampikos Kottos for stimulating discussions. This work was supported by the Air Force Office of Scientific Research and the Simons Foundation.

*Corresponding author.
aalu@gc.cuny.edu

[1] H. Hodaei, M.-A. Miri, M. Heinrich, D. N. Christodoulides, and M. Khajavikhan, Parity-time–symmetric microring lasers, Science **346**, 975 (2014).
[2] L. Feng, Z. J. Wong, R.-M. Ma, Y. Wang, and X. Zhang, Single-mode laser by parity-time symmetry breaking, Science **346**, 972 (2014).
[3] Z. Lin, H. Ramezani, T. Eichelkraut, T. Kottos, H. Cao, and D. N. Christodoulides, Unidirectional Invisibility Induced by PT-Symmetric Periodic Structures, Phys. Rev. Lett. **106**, 213901 (2011).
[4] A. Regensburger, C. Bersch, M. A. Miri, G. Onishchukov, D. N. Christodoulides, and U. Peschel, Parity-time synthetic photonic lattices, Nature (London) **488**, 167 (2012).
[5] L. Feng, Y.-L. Xu, W. S. Fegadolli, M.-H. Lu, J. E. B. Oliveira, V. R. Almeida, Y.-F. Chen, and A. Scherer,

Experimental demonstration of a unidirectional reflectionless parity-time metamaterial at optical frequencies, Nat. Mater. **12**, 108 (2013).
[6] S. Longhi, PT-symmetric laser absorber, Phys. Rev. A **82**, 031801(R) (2010).
[7] Y. D. Chong, L. Ge, and A. D. Stone, PT-Symmetry Breaking and Laser-Absorber Modes in Optical Scattering Systems, Phys. Rev. Lett. **106**, 093902 (2011).
[8] Y. Sun, W. Tan, H. Q. Li, J. Liand H. Chen, Experimental Demonstration of a Coherent Perfect Absorber with PT Phase Transition, Phys. Rev. Lett. **112**, 143903 (2014).
[9] L. Ge, Y. D. Chong, and A. D. Stone, Conservation relations and anisotropic transmission resonances in one-dimensional PT-symmetric photonic heterostructures, Phys. Rev. A **85**, 023802 (2012).
[10] R. Fleury, D. Sounas, and A. Alù, An invisible acoustic sensor based on parity-time symmetry, Nat. Commun. **6**, 5905 (2015).
[11] L. Feng, R. El-Ganainy, and L. Ge, Non-Hermitian photonics based on parity-time symmetry, Nat. Photonics **11**, 752 (2017).
[12] R. El-Ganainy, K. G. Makris, M. Khajavikhan, Z. H. Musslimani, S. Rotter, and D. N. Christodoulides, Non-Hermitian physics and PT symmetry, Nat. Phys. **14**, 11 (2018).
[13] M.-A. Miri and A. Alù, Exceptional points in optics and photonics, Science **363**, eaar7709 (2019).
[14] S. K. Özdemir, S. Rotter, F. Nori, and L. Yang, Parity–time symmetry and exceptional points in photonics, Nat. Mater. **18**, 783 (2019).
[15] D. Christodoulides and J. Yang, *Parity-Time Symmetry and Its Applications* (Springer, Berlin, 2018).
[16] A. A. Zyablovsky, A. P. Vinogradov, A. A. Pukhov, A. V. Dorofeenko, and A. A. Lisyansky, PT-symmetry in optics, Phys. Usp. **57**, 1063 (2014).
[17] C. M. Bender and S. Böttcher, Real Spectra in Non-Hermitian Hamiltonians Having PT Symmetry, Phys. Rev. Lett. **80**, 5243 (1998).
[18] C. M. Bender, D. C. Brody, and H. F. Jones, Complex Extension of Quantum Mechanics, Phys. Rev. Lett. **89**, 270401 (2002).
[19] C. M. Bender, Making sense of non-Hermitian Hamiltonians, Rep. Prog. Phys. **70**, 947 (2007).
[20] J. Schindler, A. Li, M. C. Zheng, F. M. Ellis, and T. Kottos, Experimental study of active LRC circuits with PT symmetries, Phys. Rev. A **84**, 040101(R) (2011).
[21] M. Chitsazi, H. Li, F. M. Ellis, and T. Kottos, Experimental Realization of Floquet PT-Symmetric Systems, Phys. Rev. Lett. **119**, 093901 (2017).
[22] H. Benisty *et al.* Implementation of PT symmetric devices using plasmonics: Principle and applications, Opt. Express **19**, 18004 (2011).
[23] H. Alaeian and J. A. Dionne, Parity-time-symmetric plasmonic metamaterials, Phys. Rev. A **89**, 033829 (2014).
[24] X. Zhu, H. Ramezani, C. Shi, J. Zhu, and X. Zhang, PT-Symmetric Acoustics, Phys. Rev. X **4**, 031042 (2014).
[25] M. Kang, F. Liu, and J. Li, Effective spontaneous PT-symmetry breaking in hybridized metamaterials, Phys. Rev. A **87**, 053824 (2013).
[26] R. Fleury, D. L. Sounas, and A. Alù, Negative Refraction and Planar Focusing Based on Parity-Time Symmetric Metasurfaces, Phys. Rev. Lett. **113**, 023903 (2014).
[27] M. Lawrence, N. Xu, X. Zhang, L. Cong, J. Han, W. Zhang, and S. Zhang, Manifestation of PT Symmetry Breaking in Polarization Space with Terahertz Metasurfaces, Phys. Rev. Lett. **113**, 093901 (2014).
[28] R. Fleury, D. L. Sounas, and A. Alù, Parity-time symmetry in acoustics: Theory, devices, and potential applications, IEEE J. Sel. Top. Quantum Electron. **22**, 121 (2016).
[29] H. Schomerus, Quantum Noise and Self-Sustained Radiation of PT-Symmetric Systems, Phys. Rev. Lett. **104**, 233601 (2010).
[30] G. S. Agarwal and K. Qu, Spontaneous generation of photons in transmission of quantum fields in PT-symmetric optical systems, Phys. Rev. A **85**, 031802(R) (2012).
[31] S. Scheel and A. Szameit, PT-symmetric photonic quantum systems with gain and loss do not exist, Europhys. Lett. **122**, 34001 (2018).
[32] A. Guo, G. J. Salamo, D. Duchesne, R. Morandotti, M. Volatier-Ravat, V. Aimez, G. A. Siviloglou, and D. N. Christodoulides, Observation of PT-Symmetry Breaking in Complex Optical Potentials, Phys. Rev. Lett. **103**, 093902 (2009).
[33] M. Gräfe, R. Heilmann, R. Keil, T. Eichelkraut, M. Heinrich, S. Nolte, and A. Szameit, Correlations of indistinguishable particles in non-Hermitian lattices, New J. Phys. **15**, 033008 (2013).
[34] T. Eichelkraut, R. Heilmann, S. Weimann, S. Stützer, F. Dreisow, D. N. Christodoulides, S. Nolte, and A. Szameit, Mobility transition from ballistic to diffusive transport in non-Hermitian lattices, Nat. Commun. **4**, 2533 (2013).
[35] M. Ornigotti and A. Szameit, Quasi PT-symmetry in passive photonic lattices, J. Opt. **16**, 065501 (2014).
[36] D. G. Baranov, A. Krasnok, and A. Alù, Coherent virtual absorption based on complex zero excitation for ideal light capturing, Optica **4**, 1457 (2017).
[37] A. Krasnok, D. G. Baranov, A. Generalov, S. Li, and A. Alù, Coherently Enhanced Wireless Power Transfer, Phys. Rev. Lett. **120**, 143901 (2018).
[38] G. Trainiti, Y. Radi, M. Ruzzene, and A. Alù, Coherent virtual absorption of elastodynamic waves, Sci. Adv. **5**, eaaw3255 (2019).
[39] M. Cotrufo and A. Alù, Excitation of single-photon embedded eigenstates in coupled cavity-atom systems, Optica **6**, 799 (2019).
[40] D. M. Pozar, *Microwave Engineering* (Wiley, New York, 1998).
[41] See Supplemental Material at http://link.aps.org/supplemental/10.1103/PhysRevLett.124.193901 for the analysis of the virtual PT-symmetric circuit in Fig. 2(a).
[42] W. Suh, Z. Wang, and S. Fan, Temporal coupled-mode theory and the presence of non-orthogonal modes in lossless multimode cavities, IEEE J. Quantum Electron. **40**, 1511 (2004).
[43] J. Schindler, Z. Lin, J. M. Lee, H. Ramezani, F. M. Ellis, and T. Kottos, PT-symmetric electronics, J. Phys. A **45**, 444029 (2012).
[44] S. A. Schelkunoff, The impedance concept and its application to problems of reflection, refraction, shielding and power absorption, Bell Syst. Tech. J. **17**, 17 (1938).

[45] P. Ambichl, K. G. Makris, L. Ge, Y. D. Chong, A. D. Stone, and S. Rotter, Breaking of PT Symmetry in Bounded and Unbounded Scattering Systems, Phys. Rev. X **3**, 041030 (2013).

[46] In the weak-coupling limit, the initial state, i.e., the initial current $i_L^\alpha(0) \approx -C\dot{v}_\alpha(0) - G_\alpha v_\alpha(0)$ and voltage $v_C^\alpha(0) = v_\alpha(0)$ across the inductor L and capacitor C at the α resonator, can be obtained from $|\Psi(0)$ via Eq. (5).